ELSEVIER

High-power red laser diodes grown by MOVPE

M. Zorn*, H. Wenzel, U. Zeimer, B. Sumpf, G. Erbert, M. Weyers

Materials Technology Department, Ferdinand-Braun-Institut für Höchstfrequenztechnik (FBH), Gustav-Kirchhoff-Str. 4, D-12489 Berlin, Germany

Abstract

We report on the development of high-power laser diodes and laser bars emitting in the visible red spectral region. In contrast to the normally used epitaxial structure consisting of Al(Ga)InP waveguide and cladding layers embedding an GaInP quantum well (QW) we also investigated AlGaAs as material for the cladding layers in a symmetric and in an asymmetric design. The laser performance of the different structures is compared. AlGaAs as p-cladding layer enables the use of carbon instead of zinc as p-dopand resulting in a reduced diffusion tendency of the doping material and a higher possible doping level. Furthermore, the influence of QW number and thickness on the laser performance is investigated. With optimized layer structures 5-mm wide laser bars at 650 nm with a maximal output power of 55 W in pulsed operation were realized.
© 2006 Elsevier B.V. All rights reserved.

1. Introduction

High-power laser diodes emitting in the visible red wavelength range (630–710 nm) find increasing interest e.g. for data storage, medical applications like photodynamic therapy (PDT), for pumping of solid state lasers (e.g. Cr:LiSAF/Cr:LiCAF) and display applications like laser projection. Depending on the required output power broad area devices or laser bars with very good reliability are needed.

The epitaxial layer structures usually applied consist of Al(Ga)InP cladding layers and AlGaInP waveguide layers embedding GaInP quantum wells (QW) [1]. Reliable operation of high-power laser diodes and laser bars using such a structure has been reported [2–6]. Maximum output powers are around 2 W for single emitters [2,3] and from 7 W [5] to 15 W ($T = 10\,°C$, actively cooled) [4] for laser bars. A typical value for the vertical far-field angle of these devices is 40°.

The disadvantages of using Al(Ga)InP as p-cladding layer are the low achievable doping concentration in the range of $2.5 \times 10^{17}\,\mathrm{cm}^{-3}$ [7] together with the high diffusion tendency of the dopant zinc (Zn). It was tried to overcome these problems by introducing diffusion barriers [8] or change to magnesium (Mg) as p-dopant [9], which unfortunately suffers from a memory effect in the reactor [10]. Both ideas have also been combined [11].

To overcome these limitations our approach was to replace the AlInP cladding layers by AlGaAs as demonstrated by Unger et al. [12]. We investigated the possibility of replacing the AlInP in one or both cladding layers by $Al_xGa_{1-x}As$ with a high aluminium content of $x = 0.85$. This has the advantage of higher achievable carrier concentrations and a possible replacement of Zn by carbon (C) as p-type dopant. Furthermore, laser devices can be fabricated using a standard AlGaAs-based technology.

The dependence of the laser properties on the laser wavelength and on thickness and number of QWs is investigated. Laser diodes were fabricated using single, double and triple quantum wells in the wavelength range between 634 and 705 nm. Finally, results of lasers bars

*Corresponding author. Tel.: +49 30 6392 2676; fax: +49 30 6392 2685.
E-mail address: martin.zorn@fbh.berlin.de (M. Zorn).

produced from optimized epitaxial structures for 650 nm are presented.

2. Experimental procedure

The layer structures presented here were grown by metalorganic vapor phase epitaxy (MOVPE) in a horizontal Aixtron 200/4 reactor. The sources used are trimethylgallium (TMGa), trimethyaluminium (TMAl), trimethylindium (TMIn), arsine and phosphine. Silicon (Si) from Si_2H_6 was used for n-doping. Zn from dimethylzinc (DMZn) and C from carbontetrabromide (CBr_4) were utilized for p-doping. The growth pressure was 150 mbar and a typical growth temperature was 770 °C. Epiready n+ GaAs (1 0 0) substrates misoriented 6° towards [1 1 1]A were used. The growth process was monitored using a LayTec EpiRAS 200 system [13]. The epitaxial structures were processed into broad area lasers. In pulsed regime (1 μs pulse duration, 5 kHz repetition rate) the threshold current density (j_{th}), the characteristic temperature of the threshold current density (T_0), and the vertical far field angle ($\Theta_{1/2}$) were determined from unmounted and uncoated $100\,\mu m \times 1000\,\mu m$ broad area lasers. From measurements of these values for several cavity lengths, the transparency current density (j_{TR}), the modal gain coefficient ($\Gamma^* g_0$), the internal efficiency (η_i), and the internal loss (α_i) were determined assuming a logarithmic dependence of the current density on the modal gain. Results for laser bars are shown for mounted devices as described below.

3. Results and discussion

For the epitaxial growth of visible red laser diodes three different structures were investigated. The first one is a standard structure with AlInP cladding layers and AlGaInP waveguide layers embedding the GaInP QWs. For the second structure the AlInP cladding layers were replaced by $Al_{0.85}Ga_{0.15}As$. The third structure is an asymmetric mixture of both designs consisting of n:AlInP and p:$Al_{0.85}Ga_{0.15}As$ cladding layers. Laser diodes were investigated over the whole wavelength range from 634 to 705 nm. The measured threshold current densities j_{th} are summarized in Fig. 1. We used compressively strained double QWs (DQW) in the wavelength region around 650 nm and single QWs (SQW) near 630 nm (tensile strained) and above 680 nm (compressively strained). Data for SQWs at 650 and 670 nm, respectively, are added for comparison. It can be seen that the threshold current density decreases for increasing laser wavelengths due to the increasing barrier height around the QW resulting in a better carrier confinement. However, at wavelengths above 690 nm a high amount of indium has to be incorporated into the QW. This leads to very high compressive strain in the QW and to a strong decrease in laser performance above 700 nm due to the formation of defects. Laser devices above 700 nm must be therefore realized by using
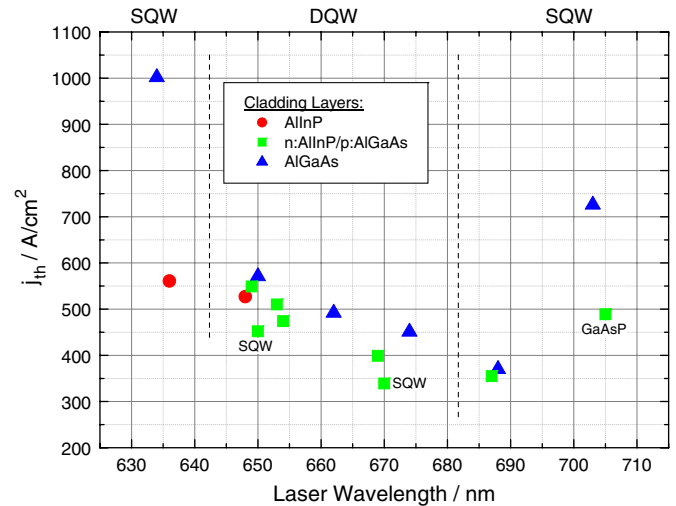

Fig. 1. Dependence of threshold current density j_{th} on laser wavelength for unmounted $100\,\mu m \times 1000\,\mu m$ broad area lasers with cladding layers as indicated. Depending on the wavelength GaInP SQWs or DQWs have been used. The laser at 705 nm features a GaAsP SQW.
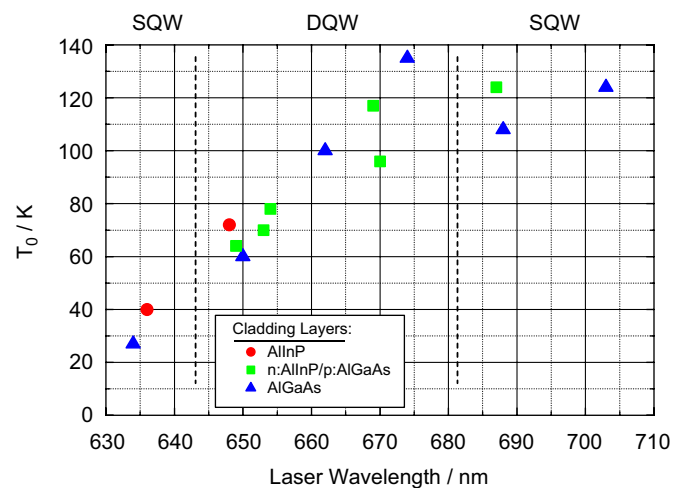

Fig. 2. Dependence of the characteristic temperature T_0 on the laser wavelength for unmounted $100\,\mu m \times 1000\,\mu m$ broad area lasers with cladding layers as indicated. Depending on the wavelength GaInP SQWs or DQWs have been used.

other QW materials. This can e.g. be done by using a GaAsP SQW as shown in Fig. 1 for 705 nm resulting in a significantly lower threshold current density as compared to the GaInP SQW at 703 nm. Comparing the laser performance around 630 nm for lasers with AlInP and AlGaAs cladding layers it can be stated that in this wavelength range the best performance can be reached with n: and p:AlInP cladding layers. In the mid-wavelength range the asymmetric structure laser has a better performance than the structure with n: and p:AlGaAs cladding layers.

A second important point for the laser performance is the temperature stability expressed by the characteristic temperature T_0 of the threshold current, which is investigated in Fig. 2. For wavelengths around 635 nm reasonable

Table 1
Comparison of room temperature laser data for broad area lasers in the 630 nm wavelength range with different thicknesses of the tensile strained SQW

d_{QW} (nm)	x_{In}	Strain	λ (nm)	I_{th} (mA)	T_0 (K)	j_{TR} (A cm^{-2})	$\Gamma^* g_0$ (cm^{-1})	η_i	α_i (cm^{-1})
8	0.40	-6.3×10^{-3}	633	780	30	340	16	0.84	2.2
10	0.38	-7.8×10^{-3}	634	590	32	310	18	0.82	0.6
13	0.36	-9.3×10^{-3}	635	600	36	340	22	0.81	0.8
15	0.35	-10.0×10^{-3}	636	560	40	320	23	0.88	1.5

The data were obtained from lasers with a cavity length of 1000 μm and from length dependent measurements (last four columns). The stripe width is 100 μm. The vertical far field angle for all structures is 35°.

Table 2
Comparison of room temperature laser data for broad area lasers with AlInP, n:AlInP/p:AlGaAs and AlGaAs cladding layers

Structure	λ (nm)	I_{th} (mA)	T_0 (K)	$\Theta_{1/2}$	j_{TR} (A cm^{-2})	$\Gamma^* g_0$ (cm^{-1})	η_i	α_i (cm^{-1})
AlInP	648	530	72	34	360	39	0.95	3.8
AlInP/AlGaAs	649	550	64	31	370	35	0.91	2.2
AlGaAs	650	570	60	29	340	26	0.81	1.7

The data were obtained from lasers with a cavity length of 1000 μm and from length dependent measurements (last four columns). The stripe width is 100 μm. All structures have a DQW.

values of 40 K can be achieved by using AlInP cladding layers while the value is only half for the structure with AlGaAs cladding layers. This again is an advantage for the AlInP cladding layers in the shortest wavelength range. With increasing wavelength the value of T_0 also increases and reaches a maximum of 135 K at 674 nm using the structure with AlGaAs cladding layers. Increasing the wavelength further leads to values around 120 K.

The active region of the lasers emitting near 630 nm consists of a tensile-strained SQW. As it is known, a careful optimization of the thickness and the strain of tensile-strained active regions can lead to a significant reduction of the threshold current [14,15]. A comparison of the laser data for QWs emitting near 630 nm having thicknesses d between 8 and 15 nm is given in Table 1. It can be seen that with increasing QW thickness the threshold current density j_{th} decreases while the characteristic temperature T_0 increases. The transparency current density remains almost constant but an increase of the modal gain coefficient $\Gamma^* g_0$ can be observed. This increase can be attributed only partially to the stronger wave guiding due to the thicker QW (according to simulation, Γ/d rises by 10%) but mainly to the increased differential gain $d^* g_0$ of the QW. This effect is caused by the enhancement of the strain with increasing thickness in order to keep the emission wavelength nearly constant (compare column 3 in Table 1), which leads to an increased splitting between the light and heavy hole sub-bands and a change in their dispersion.

For the wavelength range around 650 nm a detailed comparison of the different cladding layers is given in Table 2. The structure with the AlInP cladding layers has the lowest threshold current density j_{th} together with the highest T_0 while it is the opposite for the structure with the AlGaAs cladding layers. This can be explained by the reduced far field angle of the structure with the AlGaAs cladding layer connected to a smaller QW confinement

factor. The internal efficiency is the highest for the AlInP structure while the differential efficiency is the highest for the asymmetric structure. Additionally, it should be noted that for the AlInP structure the Zn:AlInP p-cladding layer was grown at a reduced growth temperature of 660 °C to enable a higher Zn incorporation. This leads to a better laser performance of these structures [16]. However, the reduced growth temperature leads also to a reduced crystalline quality of these layers and therefore to insufficient reliability. A good compromise is therefore the asymmetric structure enabling also a standard AlGaAs processing with the possibility of increasing the p-doping in the cladding layer. The further development of the laser devices for 650 nm was therefore based on the asymmetric structure with n:AlInP and p:Al$_{0.85}$Ga$_{0.15}$As cladding layers.

One of the main advantages of this structure is the possibility to replace Zn by C for the doping of the p-cladding layer. Fig. 3 shows Zn profiles of laser structures with different p-cladding layers taken by secondary ion mass spectroscopy (SIMS). The aluminum content is also shown as marker. Both structures consist of p:Al$_{0.85}$Ga$_{0.15}$As cladding layers. In the first structure the p-cladding layer is doped with Zn (dashed line) while in the second structure it is doped by using C (straight line). The growth of the waveguide layers in both structures was performed identically. By comparing the Zn concentration near the QW (circle) in both structures it can be seen that the Zn concentration directly at the QW can significantly be reduced if C is used for the doping of the cladding layers. This is caused by a reduced total amount of Zn in the structure resulting in a reduced diffusion tendency towards the QW. In the following all structures are therefore C doped in the AlGaAs cladding.

In the next step we investigated the influence of the QW number on the laser performance. Here we used an

optimized structure where we primarily increased the C-doping of the p:$Al_{0.85}Ga_{0.15}As$ cladding layer significantly. Table 3 shows a collection of laser data for unmounted broad area test lasers consisting of one (SQW), two (DQW), and three (TQW) QWs. It can be seen that the threshold current density j_{th} increases with increasing QW number while the thermal stability represented by T_0 is increasing for a higher number of QWs. This is caused by the fact that a higher current is necessary to pump the higher number of QWs. In our experiments it was found that the long-term stability of the lasers applying three QWs is not satisfying up to now. Final devices were therefore fabricated using either SQWs or DQWs.

At 650 nm and operated in cw operation broad area lasers having a DQW with a size of $100 \mu m \times 750 \mu m$ showed a maximum output power of nearly 1 W at 15 °C with a reliable operation over more than 6000 h at 500 mW [17]. Ten millimeter wide bars using also a DQW consisting of 19 emitters with 30 μm stripe width showed a maximal output power of 9.6 W with a lifetime of more than 1000 h at 15 °C and 4 W [18]. The vertical far field of these structures is below 32°, which is significantly smaller than usually found in literature.

To evaluate the high potential of the material presented, Fig. 4 shows the power–current characteristics together with the conversion efficiency and the driving voltage for a 5 mm wide bar with ten 100 μm stripe width lasers with a SQW emitting at 650 nm. The devices were mounted p-side down on CuW heat spreaders using AuSn solder. In pulsed operation (150 μs pulse duration, 10 Hz repetition rate, 15 °C) a maximum output power of 55 W at a current of 80 A was reached.

4. Summary

The development of epitaxial structures for laser diodes emitting in the visible red region from 630 to 710 nm is presented. For wavelength around 630 nm the best results have been achieved using AlInP cladding layers with 17 nm thick GaInP QWs. At higher wavelength a structure with n:AlInP and p:AlGaAs cladding layers shows a very good performance. In the AlGaAs cladding layers C can be used as p-dopant instead of Zn, which reduces Zn diffusion towards the QW. For wavelength above 700 nm the highly strained GaInP QWs should be replaced by GaAsP QWs. Best results around 650 nm have been achieved by using single or double QWs. Laser bars with an optimized
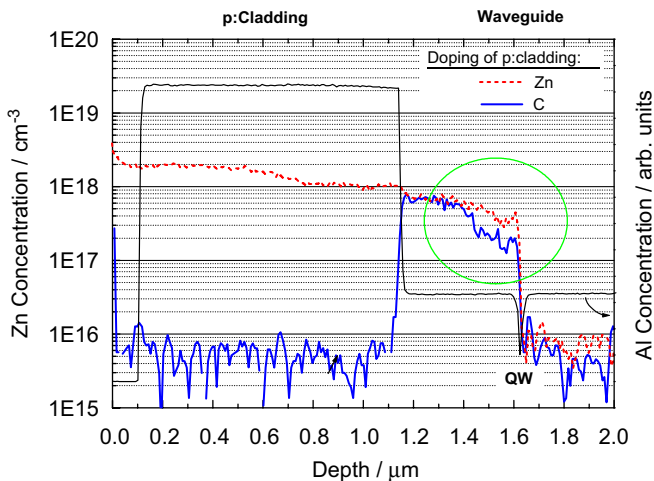

Fig. 3. SIMS profiles comparing the Zn concentration in laser structures with different p:AlGaAs (cladding) dopants: Zn (dashed) and C (straight). A reduced Zn concentration near the QW (circle) can be seen for the C doped structure.
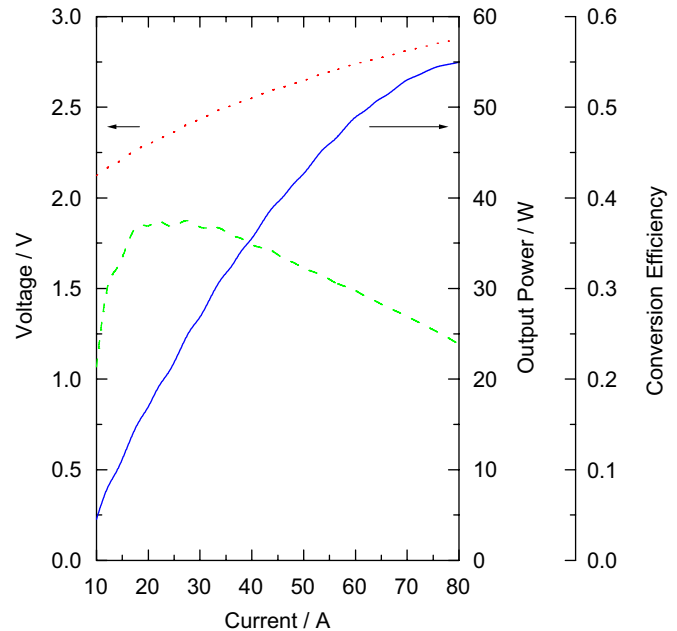

Fig. 4. Power–current characteristics (straight line) of a 10-emitter laser bar emitting at 650 nm together with the driving voltage (dotted line) and the wall plug efficiency (dashed line) at 15 °C.

Table 3
Comparison of room temperature laser data for broad area lasers using single, double and triple QWs in asymmetric n:AlInP/p:AlGaAs cladding layers

Structure	λ (nm)	I_{th} (mA)	T_0 (K)	j_{TR} (A cm^{-2})	$\Gamma^* g_0$ (cm^{-1})	η_i	α_i (cm^{-1})
SQW	652	440	55	220	18	0.83	1.0
DQW	653	510	70	300	26	0.94	2.2
TQW	654	580	83	370	34	0.98	3.6

The data were obtained from lasers with a cavity length of 1000 μm and from length dependent measurements (last 4 columns). The stripe width is 100 μm.

structure showed a maximum output power of 55 W in pulsed operation.

Acknowledgment

References

[1] D.P. Bour, R.S. Geels, D.W. Treat, T.L. Paoli, F. Ponce, R.L. Thornton, B.S. Krusor, R.D. Bringans, D.F. Welch, IEEE J. Quant. Electron. 30 (1994) 593.

[2] S. Orsila, M. Toivonen, P. Savolainen, V. Vilokkinen, P. Melanen, M. Pessa, M. Saarinen, P. Uusimaa, P. Corvini, F. Fang, M. Jansen, R. Nabiev, SPIE 3628 (1999) 203.

[3] L. Toikkanen, M. Dumitrescu, A. Tukiainen, S. Viitala, M. Suominen, V. Erojärvi, V. Rimpiläinen, R. Rönkkö, M. Pessa, SPIE 5452 (2004) 199.

[4] J.S. Osinski, B. Lu, H. Zhao, B. Schmidt, Electron. Lett. 34 (1998) 2336.

[5] D. Imanishi, Y. Sato, K. Naganuma, S. Ito, S. Hirata, Electron. Lett. 41 (2005) 1172.

[6] ⟨http://catalog.osram-os.com/media/_en/Graphics/00029998_0.pdf⟩

[7] Y. Nishikawa, Y. Tsuburai, C. Nozaki, Y. Ohba, Y. Kokubun, H. Kinoshita, Appl. Phys. Lett. 53 (1988) 2182.

[8] Y.C. Shin, B.J. Kim, D.H. Kang, Y.M. Kim, T.G. Kim, Semicond. Sci. Technol. 2 (2006) 35.

[9] T. Onishi, K. Inoue, K. Onozawa, T. Takayama, M. Yuri, IEEE J. Quant. Electron. 40 (2004) 1634.

[10] T.F. Kuech, P.-J. Wang, M.A. Tischler, R. Potemski, G.J. Scilla, F. Cardone, J. Crystal Growth 93 (1988) 624.

[11] R. Winterhoff, P. Raisch, V. Frey, W. Wagner, F. Scholz, J. Crystal Growth 195 (1998) 132.

[12] P. Unger, G.-L. Bona, R. Germann, P. Roentgen, D.J. Webb, IEEE J. Quant. Electron. 29 (1993) 1880.

[13] M. Zorn, M. Weyers, J. Crystal Growth 276 (2005) 29.

[14] A. Knauer, F. Bugge, G. Erbert, H. Wenzel, K. Vogel, U. Zeimer, M. Weyers, J. Electron. Mater. 29 (2000) 53.

[15] H. Wenzel, G. Erbert, F. Bugge, A. Knauer, J. Maege, J. Sebastian, R. Staske, K. Vogel, G. Tränkle, SPIE 3947 (2000) 32.

[16] M. Zorn, H. Wenzel, A. Knigge, U. Zeimer, M. Weyers, in: Proceedings of the 10th European Workshop on Metalorganic Vapour Phase Epitaxy, Lecce, Italy, June 2003, PS.V.09, ISBN 88-8305-007-X.

[17] B. Sumpf, M. Zorn, R. Staske, J. Fricke, P. Ressel, G. Erbert, M. Weyers, G. Tränkle, Proc. SPIE 6133 (2006) 78.

[18] B. Sumpf, M. Zorn, R. Staske, J. Fricke, P. Ressel, G. Erbert, M. Weyers, G. Tränkle, Photon. Technol. Lett. 18 (2006) 1955.